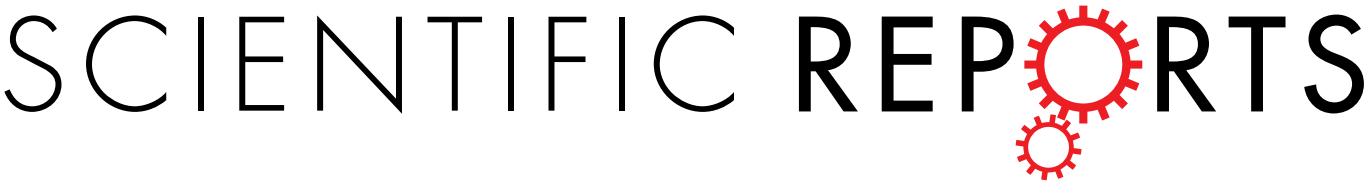

OPEN

Non-Contact Measurement of Thermal Diffusivity in Ion-Implanted Nuclear Materials

Received: 14 June 2015
Accepted: 06 October 2015
Published: 03 November 2015

F. Hofmann[1], D. R. Mason[2], J. K. Eliason[3], A. A. Maznev[3], K. A. Nelson[3] & S. L. Dudarev[2]

Knowledge of mechanical and physical property evolution due to irradiation damage is essential for the development of future fission and fusion reactors. Ion-irradiation provides an excellent proxy for studying irradiation damage, allowing high damage doses without sample activation. Limited ion-penetration-depth means that only few-micron-thick damaged layers are produced. Substantial effort has been devoted to probing the mechanical properties of these thin implanted layers. Yet, whilst key to reactor design, their thermal transport properties remain largely unexplored due to a lack of suitable measurement techniques. Here we demonstrate non-contact thermal diffusivity measurements in ion-implanted tungsten for nuclear fusion armour. Alloying with transmutation elements and the interaction of retained gas with implantation-induced defects both lead to dramatic reductions in thermal diffusivity. These changes are well captured by our modelling approaches. Our observations have important implications for the design of future fusion power plants.

Nuclear fusion is an ideal sustainable energy source. A major hurdle to its commercial development is the availability of sufficiently resilient materials. Tungsten-based alloys are the main candidates for plasma-facing components in future magnetic confinement fusion reactors[1]. In a demonstration (DEMO) reactor they will be exposed to high temperatures (~1500 K), irradiation with 14.1 MeV fusion neutrons and a large flux of energetic ions (up to 15 MWm^{-2})[2,3]. High thermal conductivity is one of the main material selection criteria[4]. A significant degradation of thermal conductivity could result in excessive temperatures with potentially disastrous consequences for fusion armour integrity[5].

Exposure of fusion armour to 14.1 MeV neutrons leads to cascade damage and transmutation alloying. Calculations indicate that after 5 years of operation, initially pure tungsten (W) in a DEMO divertor would contain up to 4 atomic % rhenium (Re)[6]. A W-5%Re alloy has less than half the room temperature thermal diffusivity of pure tungsten[7,8]. Quantifying the effects of fusion neutron cascade damage on thermal conductivity is more difficult. As a proxy, thermal transport in fission neutron irradiated tungsten has been considered[9,10]. A damage level of 0.6 displacements per atom (dpa), which would be reached in 3 months in DEMO[6], caused a reduction of room temperature thermal conductivity by 25%[10].

An interesting role is played by helium, which is formed by transmutation[6] and is also implanted from the plasma into the tungsten matrix. At elevated temperatures helium migrates from surfaces into the bulk, and strongly interacts with irradiation induced defects[11], binding to vacancies[12,13] and supressing their recombination with self-interstitial atoms (SIAs)[14]. Helium-ion implantation is an efficient tool to study this interaction[15] and great effort has been invested into the development of micro-mechanics approaches able to quantify the mechanical properties of micron-thin ion-implanted layers[16–18].

The thermal transport properties of ion-damaged layers, however, are as yet largely unexplored due to a lack of suitable experimental techniques. The references cited above used either a laser flash

[1]Department of Engineering Science, University of Oxford, Parks Road, Oxford, OX1 3PJ, UK. [2]CCFE, Culham Science Centre, Abingdon, OX14 3DB, UK. [3]Department of Chemistry, Massachusetts Institute of Technology, 77 Massachusetts Avenue, Cambridge, MA 02139, USA. Correspondence and requests for materials should be addressed to F.H. (email: felix.hofmann@eng.ox.ac.uk)

technique[8–10] or electrical resistivity measurements[7]. Both are only suited to bulk samples. Recently two new approaches, the 3-omega technique[19] and thermal reflectance measurements[20,21], have been proposed to quantify thermal transport in thin, ion-irradiated surface layers. The former required deposition of complex surface features on the sample and showed significant experimental uncertainties. The latter required samples to be coated and the probed depth depended on the, *a priori* unknown, thermal diffusivity.

Here we present a new, entirely different approach to measuring the thermal transport properties of ion-implanted materials. Using the non-contact laser-induced transient grating (TG) technique[22] we quantify thermal diffusivity in few-micron-thick layers of helium-implanted tungsten. The effect of transmutation alloying is mimicked by considering tungsten-rhenium alloys. In both types of samples we find substantial changes in thermal diffusivity. They are analysed using a kinetic theory model, providing insight into the underlying defect distribution. Our results are discussed in the light of current design practise for future fusion reactors.

Results

TG measurements use two short excitation laser pulses that are overlapped on the sample with a well-defined crossing angle (Fig. 1(a)). Interference of the pulses produces a spatially sinusoidal intensity grating with a fringe spacing λ[23]. Absorption of the light leads to a temperature grating with period λ. Rapid thermal expansion also launches two counter-propagating surface acoustic waves (SAWs)[24]. Both the thermal grating and the SAWs cause displacements of the sample surface. These are detected by diffraction of a quasi-continuous probe beam, heterodyned with a reflected reference beam (Fig. 1(b)). Fig. 1(c) presents the signal measured from a pure tungsten sample showing a number of oscillations, due to the propagating SAWs, superimposed on a background due to the decaying temperature grating.

On the surface of bulk samples thermal transport occurs both in-plane, from peaks to troughs of the thermal grating, and into the depth of the sample. The surface profile due to the thermal grating follows a non-exponential decay[23]:

$$\frac{\partial u_z}{\partial x} \propto \mathrm{erfc}\left(q\sqrt{\alpha t}\right) \tag{1}$$

Here $q = 2\pi/\lambda$, t is time and α is the isotropic thermal diffusivity, $\alpha = \kappa/C$, where κ is thermal conductivity and C the volumetric heat capacity. Thermal diffusivity is determined by fitting Eqn. 1 to the experimental data, also taking into account the sinusoidal variation due to SAWs (see supplementary sections 1 and 2). Figure 1(c) shows the fit to pure tungsten data.

TG measurements have several important advantages over previously mentioned approaches. No sample coating or indeed contact with samples is required. A well-polished sample surface that allows specular reflection of the probe and reference beams is sufficient. The probed depth is directly set by the experimental geometry. The accuracy of thermal measurements is intrinsically high since the technique does not rely on measuring a temperature difference or heat flux. Simultaneously the measurements also provide surface acoustic wave data that can be used for very sensitive measurements of elastic properties[24].

Thermal transport measurements were carried out on 99.9% pure tungsten and on tungsten rhenium alloy samples (W-1%Re, W-2%Re) to mimic the effects of transmutation alloying. Two pure tungsten samples were helium-implanted at 300 °C, using multiple ion energies to achieve approximately uniform predicted helium concentrations of 280 ± 40 atomic parts per million (appm) and 3100 ± 480 appm respectively in a 2.6 μm thick surface layer[25]. The former mimics the maximum helium concentration expected from transmutation[6], whilst the latter serves to study the effect of larger helium concentrations due to helium migration from the material surface[26]. The damage associated with the helium implantations, predicted using the Stopping Range of Ions in Matter (SRIM) code[27], was 0.017 ± 0.004 dpa and 0.19 ± 0.04 dpa respectively. Calculated implantation profiles are shown in supplementary Fig. S1.

An important question concerns the choice of the transient grating period, λ. In bulk samples TG measurements probe thermal properties up to a depth of approximately λ/π[23]. The implanted layer thickness in the helium-implanted samples is approximately 2.6 μm. To ensure that the unimplanted substrate did not affect the thermal transport measurements, a value of $\lambda = 2.74$ μm was chosen. Pure tungsten was measured at temperatures of 140 K, 200 K, 296 K, 373 K and 473 K, whilst all other samples were measured at the latter three temperatures. Figures 2 and 3 show the measured thermal diffusivities for the alloy samples and the helium-implanted samples respectively.

Discussion

The measured thermal diffusivity of tungsten alloys can be analysed using a kinetic theory model (see details in supplementary section 3). Provided we remain in the dilute alloy limit, the principal carriers of heat at or above the Debye temperature (312 K in tungsten[28]) are electrons[29]. Variations in thermal diffusivity can then be attributed to changes in the electron scattering time τ_e. According to Matthiessen's rule, the total electron scattering rate is the sum of rates of scattering from impurities, phonons and other electrons, subject to the Ioffe-Regel limit that the electron mean-free-path cannot be much smaller than the separation between atoms[30,31]. A fit of this model to our experimental data for pure tungsten is shown

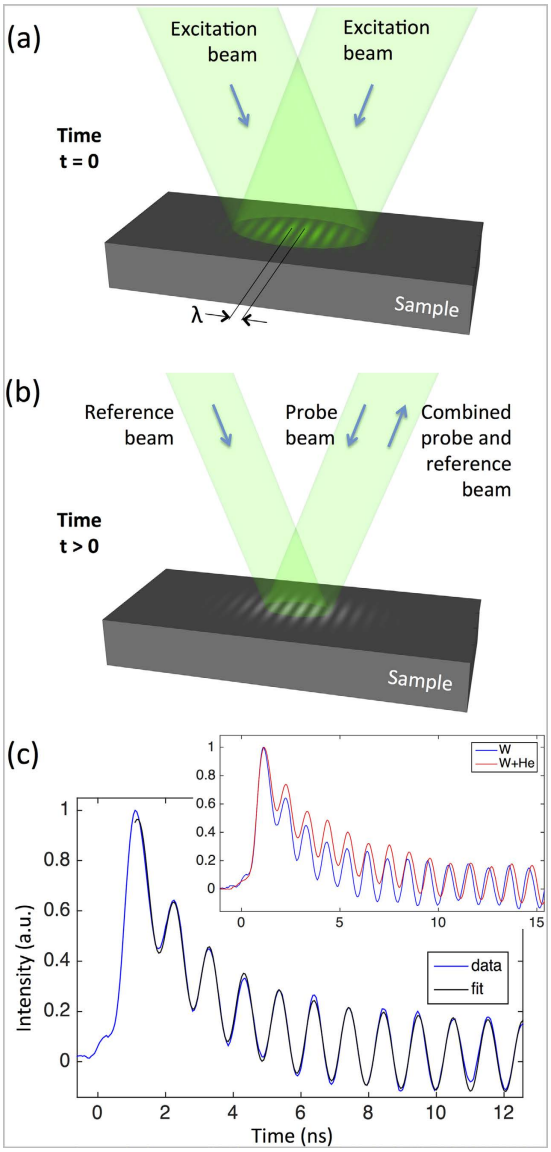

Figure 1. Transient grating thermal transport measurements. (**a**) Schematic of the measurement setup, showing the excitation beams (at time t = 0) that form the periodic transient grating light pattern (shown schematically in green) on the sample. (**b**) At time t > 0 the temperature grating and counter-propagating surface acoustic waves at the sample surface (both shown schematically in light grey) are probed. For heterodyne detection the scattered probe beam is combined with a reflected reference beam. (**c**) Experimentally recorded time trace of scattered probe intensity for the pure tungsten sample at 296 K. Also shown is a fit to the experimental data. Inset are time traces recorded for pure tungsten and tungsten implanted with 3100 appm of helium, both at 296 K. Thermal grating decay in the implanted sample is visibly slower.

in Fig. 2 (black line). Our measurements are in very good agreement with literature reference data for pure tungsten (Fig. 2 dashed line)[28,32,33] and lie within less than 10% of the data measured by Fujitsuka *et al.*[8] (also plotted in Fig. 2). This provides conclusive evidence of the reliability and accuracy of the TG technique for the contactless characterisation of thermal transport.

For the tungsten-rhenium alloys, we fit a further parameter, the scattering rate due to a rhenium atom in a tungsten matrix, finding $\sigma_{0,Re} = 1.38 \pm 0.1$ THz. We can then extrapolate to higher rhenium concentrations. Shown in Fig. 2 are lines for 5% to 25% rhenium alloys, with corresponding experimental measurements by Fujitsuka *et al.*[8]. Even though these rhenium concentrations are beyond the expected limit of validity of the dilute-alloy model, the match is surprisingly good, demonstrating that the TG technique delivers reliable and transferable thermal parameters.

At low temperatures, using the Wiedemann-Franz law[29], we can estimate that the change in resistivity due to a single rhenium atom in the tungsten matrix is $\delta\rho_{Re} = 127 \pm 10\,\mu\Omega$cm/atomic fraction. This

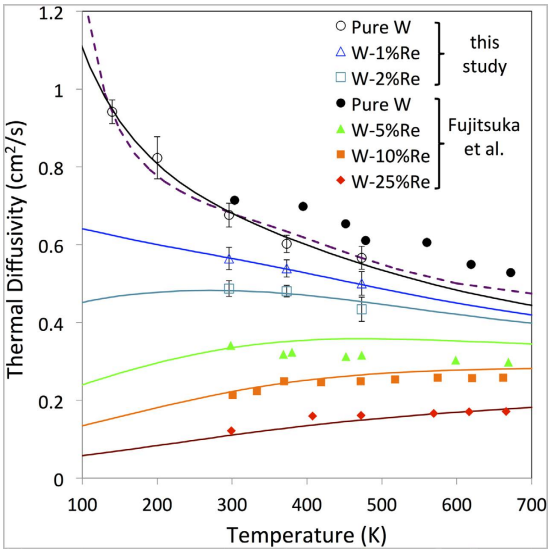

Figure 2. Thermal diffusivity of tungsten-rhenium alloys. Measured (open symbols) and modelled (solid lines) thermal diffusivity. Also shown is literature reference data for the thermal diffusivity of pure tungsten[28,32,33] (dashed purple line). The thermal diffusivity can be extrapolated from the fit to our data and compared to laser-flash measurements reported by Fujitsuka *et al.*[8] (solid symbols). Variation in the model lines due to uncertainty in the scattering rate estimate is similar to the symbol size.

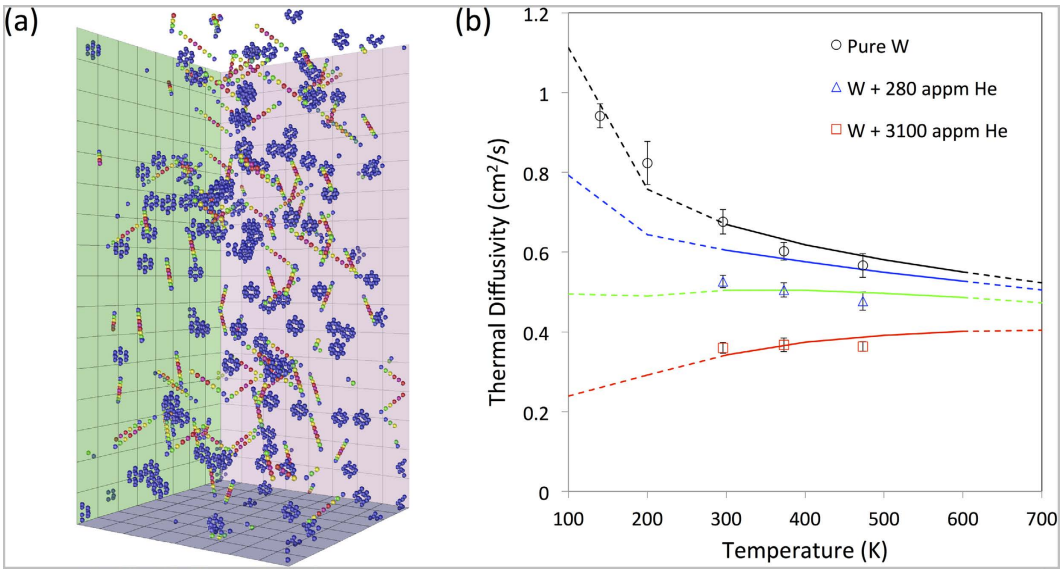

Figure 3. Thermal diffusivity of helium-implanted tungsten. (**a**) Electron scattering rates on high energy atom sites coloured blue (0.5 THz) – green – yellow – red – pink (3.5 THz) for 900 appm Frenkel pair defects in 131,000 tungsten atoms at 300 K. Vacancies are seen as blue "cages" of 8 atoms surrounding the vacant site, while interstitials are seen as ½ <111> crowdions. Bulk atoms are not shown. (**b**) Measured (open symbols) and modelled (lines) thermal diffusivity for helium-implanted tungsten. The model lines are for 0 (black), 300 (blue), 900 (green) and 3000 (red) appm Frenkel pairs in bulk tungsten. Dotted lines mark extrapolation outside the fitted temperature region.

value can be compared to the directly measured experimental value $\delta\rho_{Re} = 145\ \mu\Omega$cm/ atomic fraction[7]. Clearly the agreement is good, although our estimate is a little low as we neglected phonon conductivity in our treatment.

In the helium-implanted tungsten samples damage will be present in the form of vacancies and self-interstitials[34]. As conducting electrons can be scattered from any atom associated with a vacancy or interstitial defect, it is inappropriate to treat these defects as very strong point scatterers (see supplementary section 4). Instead we use an empirical atomistic model to estimate thermal conductivity for

the damaged layer[31] (see supplementary section 5). This model computes electron-phonon scattering locally at each atomic site and the larger contribution from Mott-Jones impurity scattering at atoms with significantly more energy than the thermal average. The total scattering due to a helium-filled vacancy is likely to be very similar to that for an empty monovacancy, as the helium atoms do not contribute valence electrons[35]. Hence this atomistic model is fitted only to the measured conductivity of pure tungsten in the range 300–600 K[28] and the resistivity per Frenkel pair[36]. The scattering rate on atomic sites is shown in Fig. 3(a), highlighting the distributed nature of scattering due to vacancy and interstitial defects.

At the implantation temperature of 573 K, vacancy mobility is low and no significant vacancy clustering and bubble growth is expected[37,38]. However, it is difficult to exactly quantify the number of interstitials and vacancies retained in the sample after implantation at finite temperature. Damage calculations using SRIM[27] indicate that approximately 60 Frenkel pairs are formed per injected helium, most of which recombine almost immediately after generation. The changes we observe are due to the few residual defects that have not recombined. Therefore we modelled thermal diffusivity for a range of Frenkel pair concentrations (Fig. 3(b)). Curves predicted for 900 appm and 3000 appm Frenkel pairs provide a good fit to the experimental data for low (280 appm) and high helium dose (3100 appm) implanted samples respectively. The helium to vacancy ratio of ~1:3 at the lower implantation dose can be compared to the value of 1:5 calculated by Becquart[39], who pointed out that at low helium doses defect retention is dominated by impurities, most notably carbon. In the present tungsten samples carbon is present at a concentration of ~900 appm. At the higher implantation dose the helium to vacancy ratio approaches 1:1 as the relative importance of impurities decreases and Frenkel pair recombination is predominantly hindered by helium occupying vacancies[24].

The measured room temperature thermal diffusivity in the high helium dose sample ($0.36\,cm^2s^{-1}$) can also be compared to that of other samples with similar levels of cascade damage (~0.2 dpa). In neutron irradiated tungsten (623 K, 0.2 dpa) thermal diffusivity was much higher ($0.60\,cm^2s^{-1}$)[9], whilst in Cu-ion implanted tungsten (298 K, 0.2 dpa), a significantly lower value was measured ($0.29\,cm^2s^{-1}$)[19]. This suggests that the calculated dpa does not provide a reliable guide to the change in thermal transport properties. This is particularly the case since retained gas and impurities clearly play a central role in determining defect removal/annihilation rates.

In conclusion we have demonstrated the feasibility of high fidelity thermal transport measurements in micron-thick ion-implantation-damaged surface layers. Our approach opens the door to a comprehensive characterisation of thermal transport properties in ion-implanted materials. The transient grating technique requires no physical contact, making it ideal for the characterisation of radioactive samples and *in situ* measurements. We have shown that the change in thermal diffusivity is not a trivial function of ion fluence and can offer an insight into the post-implantation microstructural evolution of defects invisible in transmission electron microscopy. At present the degradation of thermal transport properties due to irradiation damage is not taken into account in the design of DEMO divertor armour[40,41]. Given the substantial reductions in thermal diffusivities we have measured, it seems essential that these effects be considered in future design iterations.

Methods

Sample preparation. Tungsten and tungsten-rhenium samples were produced by arc melting of high purity elemental powders (99.9%). The resulting slugs were sectioned and mechanically polished, finishing with a colloidal silica polishing step to produce a high quality surface finish. Optical microscopy showed grains up to 1 mm in size. Electron-backscatter diffraction showed no significant texture. Tungsten samples were helium-ion-implanted at the National Ion Beam Centre, University of Surrey, UK using 12 different ion energies from 0.05 MeV to 1.8 MeV[25]. Implantation and collision damage profiles (supplementary Fig. S1) were calculated using the Stopping Range of Ions in Matter code[27] with a tungsten displacement energy of 68 eV.

Transient grating measurements. Two short excitation pulses (515 nm wavelength, 60 ps pulse duration and 1.75 μJ pulse energy) were used to generate the transient grating (Fig. 1(a)). Most measurements were performed using a grating period $\lambda = 2.74\,\mu m$, with some confirmation measurements in pure tungsten using $\lambda = 9\,\mu m$ also. Deviation of the actual grating period from the nominal value was negligible (less than 0.5%), confirmed by comparing the measured surface acoustic wave velocity in tungsten to the literature value[24]. Temperature grating decay and surface acoustic waves were probed by diffraction of a quasi-continuous probe beam (532 nm wavelength, 10 mW average power). The diffracted beam was heterodyned with a reflected reference beam (Fig. 1(b)) and the combined beam directed to a fast avalanche photo-diode. Time traces were recorded on an oscilloscope. The bandwidth of the detection system was approximately 2 GHz. Excitation and probe spot sizes of 500 μm and 150 μm diameter respectively at $1/e^2$ intensity level were used. All measurements were carried out in a cryostat (http://www.janis.com) under medium vacuum (10^{-2} mbar). The maximum measurement temperature (473 K) was imposed by the limitations of the available heating stage. There is no intrinsic limitation to the temperatures at which transient grating measurements can be performed.

References

1. Rieth, M. *et al.* Recent progress in research on tungsten materials for nuclear fusion applications in Europe. *Journal of Nuclear Materials* **432,** 482–500, doi: 10.1016/j.jnucmat.2012.08.018 (2013).
2. Maisonnier, D. *et al.* Power plant conceptual studies in Europe. *Nuclear Fusion* **47,** 1524, doi: 10.1088/0029-5515/47/11/014 (2007).
3. Asakura, N. *et al.* A simulation study of large power handling in the divertor for a Demo reactor. *Nuclear Fusion* **53,** 123013, doi: 10.1088/0029-5515/53/12/123013 (2013).
4. Rieth, M. *et al.* Review on the EFDA programme on tungsten materials technology and science. *Journal of Nuclear Materials* **417,** 463–467, doi: 10.1016/j.jnucmat.2011.01.075 (2011).
5. Norajitra, P. *et al.* Progress of He-cooled divertor development for DEMO. *Fusion Engineering and Design* **86,** 1656–1659, doi: 10.1016/j.fusengdes.2010.12.005 (2011).
6. Gilbert, M. R., Dudarev, S. L., Zheng, S., Packer, L. W. & Sublet, J.-C. An integrated model for materials in a fusion power plant: transmutation, gas production, and helium embrittlement under neutron irradiation. *Nuclear Fusion* **52,** 083019, doi: 10.1088/0029-5515/52/8/083019 (2012).
7. Tanno, T. *et al.* Effects of transmutation elements on the microstructural evolution and electrical resistivity of neutron-irradiated tungsten. *Journal of Nuclear Materials* **386–388,** 218–221, doi: 10.1016/j.jnucmat.2008.12.091 (2009).
8. Fujitsuka, M., Tsuchiya, B., Mutoh, I., Tanabe, T. & Shikama, T. Effect of neutron irradiation on thermal diffusivity of tungsten–rhenium alloys. *Journal of Nuclear Materials* **283–287, Part 2**, 1148–1151, doi: 10.1016/S0022-3115(00)00170-7 (2000).
9. Roedig, M. *et al.* Post irradiation testing of samples from the irradiation experiments PARIDE 3 and PARIDE 4. *Journal of Nuclear Materials* **329–333, Part A**, 766–770, doi: 10.1016/j.jnucmat.2004.04.176 (2004).
10. Peacock, A. T. *et al.* Overview of recent European materials R&D activities related to ITER. *Journal of Nuclear Materials* **329–333, Part A**, 173–177, doi: 10.1016/j.jnucmat.2004.04.008 (2004).
11. Yoshida, N. Review of recent works in development and evaluation of high-Z plasma facing materials. *Journal of Nuclear Materials* **266–269,** 197–206, doi: 10.1016/S0022-3115(98)00817-4 (1999).
12. Debelle, A. *et al.* Helium behaviour and vacancy defect distribution in helium implanted tungsten. *Journal of Nuclear Materials* **362,** 181–188, doi: 10.1016/j.jnucmat.2007.01.021 (2007).
13. Fu, C.-C. & Willaime, F. Ab initio study of helium in α-Fe: Dissolution, migration, and clustering with vacancies. *Physical Review B* **72,** 064117, doi: 10.1103/PhysRevB.72.064117 (2005).
14. Lucas, G. & Schäublin, R. Helium effects on displacement cascades in α-iron. *Journal of Physics: Condensed Matter* **20,** 415206, doi: 10.1088/0953-8984/20/41/415206 (2008).
15. Kornelsen, E. V. The interaction of injected helium with lattice defects in a tungsten crystal. *Radiation Effects* **13,** 227–236, doi: 10.1080/00337577208231184 (1972).
16. Kiener, D. *et al.* Application of small-scale testing for investigation of ion-beam-irradiated materials. *Journal of Materials Research* **27,** 2724–2736, doi: 10.1557/jmr.2012.303 (2012).
17. Hardie, C. D., Roberts, S. G. & Bushby, A. J. Understanding the effects of ion irradiation using nanoindentation techniques. *Journal of Nuclear Materials* **462,** 391–401, doi: 10.1016/j.jnucmat.2014.11.066 (2015).
18. Armstrong, D. E. J. *et al.* Small-scale characterisation of irradiated nuclear materials: Part II nanoindentation and micro-cantilever testing of ion irradiated nuclear materials. *Journal of Nuclear Materials* **462,** 374–381, doi: 10.1016/j.jnucmat.2015.01.053 (2015).
19. Dechaumphai, E. *et al.* Near-surface thermal characterization of plasma facing components using the 3-omega method. *Journal of Nuclear Materials* **455,** 56–60, doi: 10.1016/j.jnucmat.2014.03.059 (2014).
20. Khafizov, M., Yablinsky, C., Allen, T. R. & Hurley, D. H. Measurement of thermal conductivity in proton irradiated silicon. *Nuclear Instruments and Methods in Physics Research Section B: Beam Interactions with Materials and Atoms* **325,** 11–14, doi: 10.1016/j.nimb.2014.02.003 (2014).
21. Pakarinen, J. *et al.* Microstructure changes and thermal conductivity reduction in UO2 following 3.9 MeV He2+ ion irradiation. *Journal of Nuclear Materials* **454,** 283–289, doi: 10.1016/j.jnucmat.2014.07.053 (2014).
22. Eichler, H. J., Günter, P. & Pohl, D. W. *Laser-Induced Dynamic Gratings*. Vol. 50 (Springer-Verlag, 1986).
23. Käding, O. W., Skurk, H., Maznev, A. A. & Matthias, E. Transient thermal gratings at surfaces for thermal characterization of bulk materials and thin films. *Appl. Phys. A* **61,** 253–261, doi: 10.1007/BF01538190 (1995).
24. Hofmann, F. *et al.* Lattice swelling and modulus change in a helium-implanted tungsten alloy: X-ray micro-diffraction, surface acoustic wave measurements, and multiscale modelling. *Acta Materialia* **89,** 352–363, doi: 10.1016/j.actamat.2015.01.055 (2015).
25. Beck, C. E., Roberts, S. G., Edmondson, P. D. & Armstrong, D. E. J. Effect of Alloy Composition & Helium ion-irradiation on the Mechanical Properties of Tungsten, Tungsten-Tantalum & Tungsten-Rhenium for Fusion Power Applications. *MRS Online Proceedings Library* **1514,** 99–104, doi: 10.1557/opl.2013.356 (2013).
26. DeBroglie, I., Beck, C., Liu, W. & Hofmann, F. Temperature Dependence of Helium-ImplantationInduced Lattice Swelling in Polycrystalline Tungsten: X-ray Micro-Diffraction and Eigenstrain Modelling. *Scripta Materialia* **107,** 4, doi: 10.1016/j.scriptamat.2015.05.029 (2015).
27. Ziegler, J. F., Ziegler, M. D. & Biersack, J. P. SRIM - The stopping and range of ions in matter (2010). *Nuclear Instruments and Methods in Physics Research, Section B: Beam Interactions with Materials and Atoms* **268,** 1818–1823, doi: 10.1016/j.nimb.2010.02.091 (2010).
28. Ho, C. Y., Powell, R. W. & Liley, P. E. Thermal Conductivity of the Elements. *Journal of Physical and Chemical Reference Data* **1,** 279–421, doi: 10.1063/1.3253100 (1972).
29. Ziman, J. M. Electrons and Phonons: The Theory of Transport Phenomena in Solids. (Oxford University Press, 2001).
30. Wiesmann, H. *et al.* Simple Model for Characterizing the Electrical Resistivity in A-15 Superconductors. *Physical Review Letters* **38,** 782–785, doi: 10.1103/PhysRevLett.38.782 (1977).
31. Mason, D. R. Incorporating non-adiabatic effects in Embedded Atom potentials for radiation damage cascade simulations. *Journal of Physics: Condensed Matter* **27,** doi: 10.1088/0953-8984/27/14/145401 (2015).
32. White, G. K. & Collocott, S. J. Heat Capacity of Reference Materials: Cu and W. *Journal of Physical and Chemical Reference Data* **13,** 1251–1257, doi: 10.1063/1.555728 (1984).
33. Nix, F. C. & MacNair, D. The Thermal Expansion of Pure Metals. II: Molybdenum, Palladium, Silver, Tantalum, Tungsten, Platinum, and Lead. *Physical Review* **61,** 74–78, doi: 10.1103/PhysRev.61.74 (1942).
34. Lhuillier, P. E. *et al.* Trapping and release of helium in tungsten. *Journal of Nuclear Materials* **416,** 13–17, doi: 10.1016/j.jnucmat.2010.12.042 (2011).
35. Nguyen-Manh, D. & Dudarev, S. L. Trapping of He clusters by inert-gas impurities in tungsten: First-principles predictions and experimental validation. *Nuclear Instruments and Methods in Physics Research Section B: Beam Interactions with Materials and Atoms* **352,** 86–91, doi: 10.1016/j.nimb.2014.11.097 (2015).
36. Ullmaier, H. *Atomic Defects in Metals*. Vol. 25 (Springer-Verlag, 1991).
37. Rasch, K. D., Siegel, R. W. & Schultz, H. Quenching and recovery investigations of vacancies in tungsten. *Philosophical Magazine A* **41,** 91–117, doi: 10.1080/01418618008241833 (1980).

38. Sharafat, S., Takahashi, A., Nagasawa, K. & Ghoniem, N. A description of stress driven bubble growth of helium implanted tungsten. *Journal of Nuclear Materials* **389,** 203–212, doi: 10.1016/j.jnucmat.2009.02.027 (2009.).
39. Becquart, C. S. & Domain, C. An object Kinetic Monte Carlo Simulation of the dynamics of helium and point defects in tungsten. *Journal of Nuclear Materials* **385,** 223–227, doi: 10.1016/j.jnucmat.2008.11.027 (2009).
40. Reiser, J. & Rieth, M. Optimization and limitations of known DEMO divertor concepts. *Fusion Engineering and Design* **87,** 718–721, doi: 10.1016/j.fusengdes.2012.02.010 (2012).
41. Li-Puma, A. *et al.* Potential and limits of water cooled divertor concepts based on monoblock design as possible candidates for a DEMO reactor. *Fusion Engineering and Design* **88,** 1836–1843, doi: 10.1016/j.fusengdes.2013.05.114 (2013).

Acknowledgements

We are grateful to C.E. Beck for preparing the samples and N. Peng for carrying out the ion implantation. FH acknowledges funding from the John Fell fund (122/643) and the Royal Society (RG130308). Transient grating measurements at MIT were supported as part of the S3TEC Energy Frontier Research Center funded by the U.S. Department of Energy, Office of Basic Energy Sciences under award no. DE-SC0001299/DE-FG02-09ER46577. In part this work has been carried out within the framework of the EUROfusion Consortium and has received funding from the Euratom research and training programme 2014–2018 under grant agreement no. 633053. To obtain further information on the data and models underlying this paper please contact PublicationsManager@ccfe.ac.uk. The views and opinions expressed herein do not necessarily reflect those of the European Commission. This work was part-funded by the United Kingdom Engineering and Physical Sciences Research Council via programme grants EP/G050031 and EP/H018921/1.

Author Contributions

F.H. designed the experiments. F.H. and J.K.E. carried out the measurements. F.H. and D.R.M. carried out the data analysis and modelling. F.H., D.R.M. and J.K.E. wrote the paper. A.A.M., K.A.N. and S.L.D. read and commented on the manuscript.

Additional Information

Supplementary information accompanies this paper at http://www.nature.com/srep

Competing financial interests: The authors declare no competing financial interests.

How to cite this article: Hofmann, F. *et al.* Non-Contact Measurement of Thermal Diffusivity in Ion-Implanted Nuclear Materials. *Sci. Rep.* **5**, 16042; doi: 10.1038/srep16042 (2015).

This work is licensed under a Creative Commons Attribution 4.0 International License. The images or other third party material in this article are included in the article's Creative Commons license, unless indicated otherwise in the credit line; if the material is not included under the Creative Commons license, users will need to obtain permission from the license holder to reproduce the material. To view a copy of this license, visit http://creativecommons.org/licenses/by/4.0/